

Contents lists available at ScienceDirect

# Colloids and Surfaces A: Physicochemical and Engineering Aspects

journal homepage: www.elsevier.com/locate/colsurfa





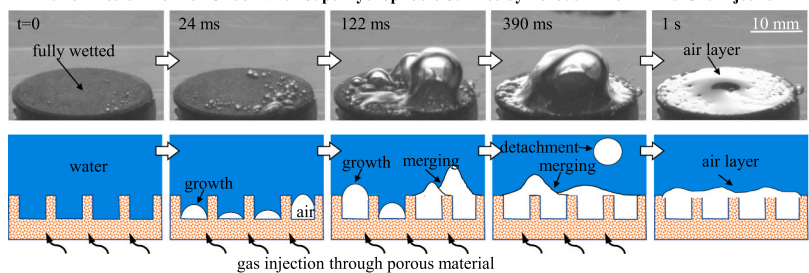
# Plastron restoration for underwater superhydrophobic surface by porous material and gas injection

Jordan Breveleri<sup>a</sup>, Shabnam Mohammadshahi<sup>a</sup>, Theresa Dunigan<sup>b</sup>, Hangjian Ling<sup>a,\*</sup>

- Department of Mechanical Engineering, University of Massachusetts Dartmouth, Dartmouth, MA 02747, USA
- <sup>b</sup> Department of Physics and Engineering, Community College of Rhode Island, Warwick, RI 02886, USA

### GRAPHICAL ABSTRACT

#### Plastron Restoration for Underwater Superhydrophobic Surface by Porous Material and Gas Injection



## ARTICLE INFO

### Keywords: Superhydrophobic surface Plastron restoration Gas injection Bubble formation Porous material

### ABSTRACT

Restoring and maintaining the gas layer (plastron) on underwater superhydrophobic surface (SHS) is critical for the real-world application of SHS, such as reducing friction drag in high-Reynolds number turbulent flows. In this work, we experimentally investigated the capability of a technology based on porous material and gas injection to restore the plastron on an underwater SHS from a fully wetted state. The SHS was created by sprayed coating a commercial superhydrophobic coating on a porous steel plate. In the experiments, the SHS was immersed in stationary liquid, the gas injection pressure and gas injection duration were independently controlled. The status of gas layer on SHS was examined by a high-speed camera. We found that the surface area being restored with a plastron increased with increasing gas injection pressure and gas injection duration, and that the plastron restoration process involved bubble formation, merging and detachment. A layer of gas was left on the surface after bubble detachment. The size of the detached bubble increased with time due to bubble merging, and became stable when there was no more bubble merging. Increasing gas injection pressure led to higher gas flow rates, larger detached bubble sizes and faster plastron restorations. A plastron restoration within 0.3 s was achieved at the highest pressure, faster than the in-situ gas generation methods. Furthermore, we found that the gas flow rate through the underwater SHS can be described by a modified Darcy's law. Our results highlighted the potential of using porous material and gas injection to restore the plastron and made possible the real-world implementation of SHS.

E-mail address: hling1@umassd.edu (H. Ling).

 $<sup>^{\</sup>star}$  Corresponding author.

### 1. Introduction

Superhydrophobic surface (SHS), inspired from the lotus effect in nature, has a wide range of underwater applications, from reducing friction drag in laminar and turbulent flows [1–4] to protecting submerged surfaces against corrosion and bio-fouling [5,6]. Furthermore, recent studies [7–10] showed that SHS can be applied to resist moisture and improve the accuracy of sensor in human health monitoring. However, implementing SHS in real-world engineering systems, e.g., on a marine ship, remains a huge challenge [11]. One of the main reason is the low stability of the gas (or plastron) trapped between the SHS and the liquid [12,13]. The gas layer, which most of SHS functions rely upon, could be unfortunately depleted due to a number of factors such as flow-induced shear [14–16] and pressure forces [17–19], gas dissolutions when exposed to undersaturated liquid [20–22], and increases of hydrostatic pressure [23–26].

In the past few years, a number of passive and active methods were explored to enhance the stability of the plastron for underwater SHS. Passive methods mainly involved the use of complex texture geometries, such as a combination of micro and nano-scale roughness (i.e., hierarchical structures) [27–32], "re-entrance" geometry [33,34], hydrophilic barriers [18], porous structures [35], and complex structures inspired from nature such as Salvinia leaves [36,37]. Many active methods based on gas replenishment were developed to sustain or restore the underwater plastron. As shown in Fig. 1, the plastron restoration means that a SHS transitions from the Wenzel state [38] where water fills the gaps between roughness elements to the Cassie-Baxter state [39] where gas fills the gaps and a gas-liquid interface forms at the tips of roughness elements. Depending on the source of the gas, these active methods can be broadly classified into five categories: (i) in-situ gas generation based on the decomposition of water [40-42] or other chemicals added in the water [43]; (ii) gas transfer from super-saturated liquid to SHS [20,44, 45]; (iii) in-situ water vapor generation by heating [46,47]; and (iv) gas injection through a single hole into the boundary layer over SHS [48, 49]; and (v) gas injection through a gas permeable material (e.g., polydimethylsiloxane surface [50]) or a porous base [51-54].

Among these active gas replenishment techniques, the one based on gas injection and porous material has advantages such as the relative ease of implementation and a capability to scale to large surface areas. Moreover, by varying the pressure difference on two sides of the porous material, this technique allowed the control of the rate of gas replenishment to match with the varying gas depletion rates under different flow conditions [50]. However, previous studies mainly focused on the effect of gas injection on the sustainability of the plastron, such as against the gas dissolution in undersaturated flows [50], against the shear and pressure forces in turbulent flows [51,52], and against the hydrostatic pressure [53]. Whether and how the gas injection technique can restore the plastron from a state where all the gas on SHS is removed (or from a fully wetted state) remains an open question. The plastron restoration has been observed with other active gas replenishment techniques, for example, these relying on in-situ gas generation [40,43]. But no experiments have been performed to demonstrate the plastron restoration capability by the gas injection technique.

In this study, we will provide the first experimental demonstration of plastron restoration by the gas injection technique. In addition, the

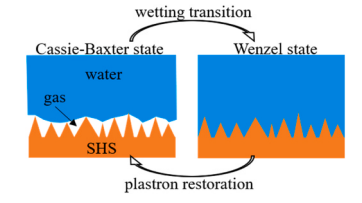


Fig. 1. Schematic showing the wetting transition and plastron restoration for the underwater SHS.

novel part of this work will include: (1) development of a new method to create SHS on porous material; and (2) understanding of *how* the plastron is restored during the gas injection process, including the time required for the plastron to be restored, and the impact of gas injection pressure and gas injection duration on the plastron restoration. Understanding the dynamic process of plastron restoration is critical for the design and implementation of the gas injection technique. For example, such knowledge could inform the pressure and the duration of gas injection. We will test the hypothesis that the success of plastron restoration depends on the gas injection pressure and gas injection duration.

## 2. Experimental methods

We created SHS on porous material by a procedure illustrated in Fig. 2(a). First, a porous disk with a diameter of 25.4 mm made of 316L stainless-steel (McMaster Carr, #9446T34, thickness 1.59 mm, porosity of 20-25 %) was cleaned and dried. A Scanning Electron Microscopy (SEM) image of the porous disk was shown in Fig. 2(b). The pore size measured from the SEM image ranged from 10 to 50 µm. Then, we sprayed a commercial superhydrophobic coating (UltraEver Dry) on one side of the porous plate. The application of UltraEver Dry coating involved two steps: a bottom coat for generating surface roughness, and a top coat for altering the surface hydrophobic chemistry. SEM images of the porous plate after applying the superhydrophobic coating were shown in Fig. 2(c-d). Clearly, after the coating, the surface consisted of both micro and nano-scale surface roughness. A number of micro-pores were not entirely covered by the coating materials, which provided pathways for the gas to pass through the surface. As shown in Fig. 2(e), the water contact angle of the coated porous disk was 162°, confirming that the surface was superhydrophobic. As shown in Fig. 2(f), when immersed in water, the entire disk was covered by a thin air layer (the fraction of surface area covered was close to 1).

To characterize how well air could pass through the fabricated sample, we experimentally measured the flow rate of air (Q) as a function of pressure difference  $(\Delta p)$  on two sides of the sample. During the measurement, both sides of the porous material were exposed to air. The pressure difference was measured by a differential pressure transmitter (Omega Engineering, #PX3005–160WDWBI, range 80 kPa, precision 0.075 %). The flow rate was measured by counting the time required to displace a specific amount of water (300 ml) by the air at the exit of porous material. Fig. 3 shows the measured Q as a function of  $\Delta p$  for the porous material before and after applying the superhydrophobic coating. As expected, for both cases, Q followed a nearly linear relationship with  $\Delta p$ . According to the Darcy's law, the flow rate passing through a porous medium can be expressed as [55]:

$$Q = \frac{kA}{\mu} \frac{\Delta p}{L},\tag{1}$$

where k is the permeability of the porous medium (SI unit m<sup>2</sup> [55]), A is the surface area (SI unit m<sup>2</sup>),  $\mu$  is the dynamic viscosity of the fluid (SI unit kg/m/s), and L is the thickness of the porous material (SI unit m). Given the SI units of Q and  $\Delta p$  as m<sup>3</sup>/s and Pa, respectively, the SI unit for k (i.e., m<sup>2</sup>) can be derived from Eq. (1). The larger the permeability, the easier the fluids can flow through the porous material. By fitting the two curves in Fig. 3, we found an air permeability of  $k = 5.5 \times 10^{-13}$  m<sup>2</sup> and  $k = 2.7 \times 10^{-14}$  m<sup>2</sup> for the porous material before and after applying the coating, respectively. As expected, the permeability reduced due to the addition of coating on the porous material.

To study the plastron restoration by gas injection, we performed experiments in an acrylic tank as shown in Fig. 4. The fabricated porous SHS was installed at the bottom of a tank, with the coated side facing to the water and the uncoated side connecting to an air compressor and a vacuum pump. The height of water in the tank was fixed at 0.15 m. The water surface was exposed to atmosphere. The air compressor aimed to replenish the plastron by injecting air upward through the porous

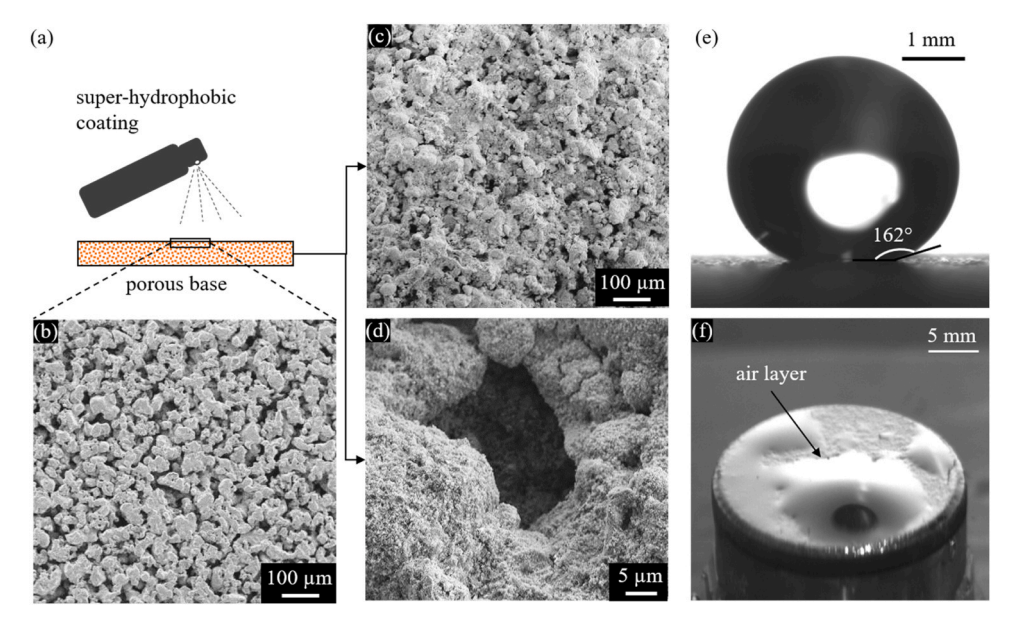
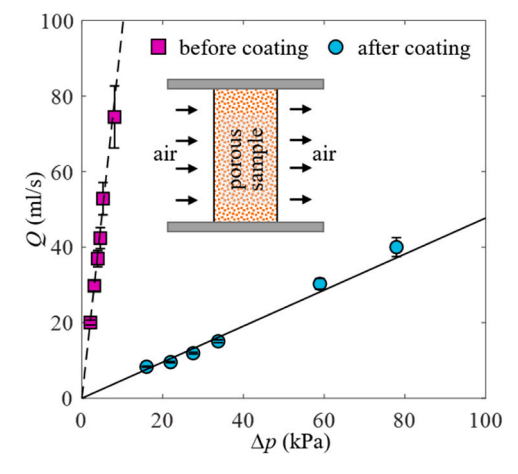
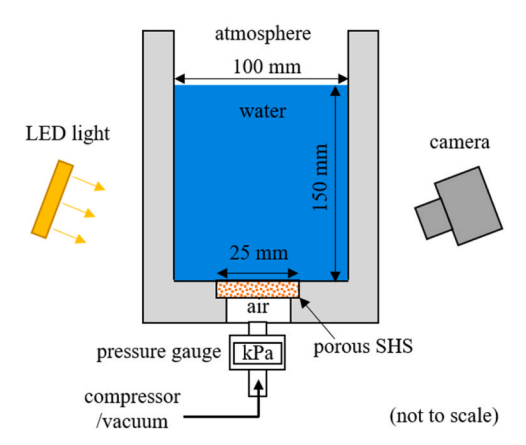


Fig. 2. (a) Schematic of fabrication procedure for creating SHS on a porous base; (b–d) SEM images of the porous plate before (b) and after (c-d) applying the superhydrophobic coating; (e) A water droplet seated on the coated plate showing a high-water contact angle; and (f) Presence of air layer on the SHS when submerged underwater.



**Fig. 3.** Flow rate of air passing through the porous material before and after applying the superhydrophobic coating. Data was collected when both sides of the porous material were exposed to air.



 ${\bf Fig.~4.}$  Experimental setup for studying the plastron restoration on a porous SHS by gas injection.

material, and the vacuum pump removed the trapped air on SHS via suction. In this work, we mainly studied the impacts of two parameters on the plastron restoration: (i) the pressure difference across the porous SHS denoted as  $\Delta p$  (a positive  $\Delta p$  indicated that air is forced upward through the SHS), and (ii) the time duration of gas injection denoted as  $\Delta t$ . To control  $\Delta p$ , we used a high-precision air regulator (McMaster Carr, #1888K1, range 25 psi) to vary the pressure at the bottom of the SHS. The magnitude of  $\Delta p$  was measured by a high precision pressure gauge (Omega Engineering, #DPG108-030 G, range 30 psi, precision 0.25 %). To control  $\Delta t$ , we used a valve (McMaster Carr, #3976T1) whose opening duration can be programmed between 1 and 10 s. To visualize the status of gas layer on SHS, we used a CMOS camera (FLIR, #GS3-U3-41C6M-C, 2048 by 2048 pixels) and a LED light located on two sides of the tank. The light illuminated the surface at an angle such that a total internal reflection occurred at the air-water interface. To capture the dynamic process of plastron depletion or restoration, we recorded images at 82 frames per second (fps).

Before each plastron restoration test, we removed all the gas on SHS by opening the vacuum pump for a short duration of about 1 s Fig. 5 shows a typical plastron depletion process. Clearly, the gas layer initially attached to the SHS was quickly removed, causing the SHS to reach a fully wetted state. After achieving the fully wetted state, the plastron restoration was tested by gas injection with different magnitudes of  $\Delta p$  and  $\Delta t$ .

### 3. Results and discussion

# 3.1. Impact of pressure and duration of gas injection on plastron restoration

We first tested whether the plastron could be restored at different magnitudes of  $\Delta p$  and  $\Delta t$ . We performed experiments for  $\Delta p$  varying from 10 to 81 kPa and  $\Delta t$  from 1 to 10 s. For each case, we captured an image of the SHS shortly after the gas injection stopped and the surface status was stable. The results are shown in Fig. 6(a). For small  $\Delta p$  and  $\Delta t$ , the plastron was only restored over a small portion of the entire surface. Instead of forming a uniform layer, isolated gas bubbles appeared on the surface. Increasing either  $\Delta p$  or  $\Delta t$  resulted in a larger surface area being recovered with the gas layer or gas bubbles. When  $\Delta p$  or  $\Delta t$  was sufficient large, the plastron on the entire surface was fully restored. In some

Fig. 5. Time-series of images showing the plastron depletion due to the gas suction from the bottom of the porous surface.

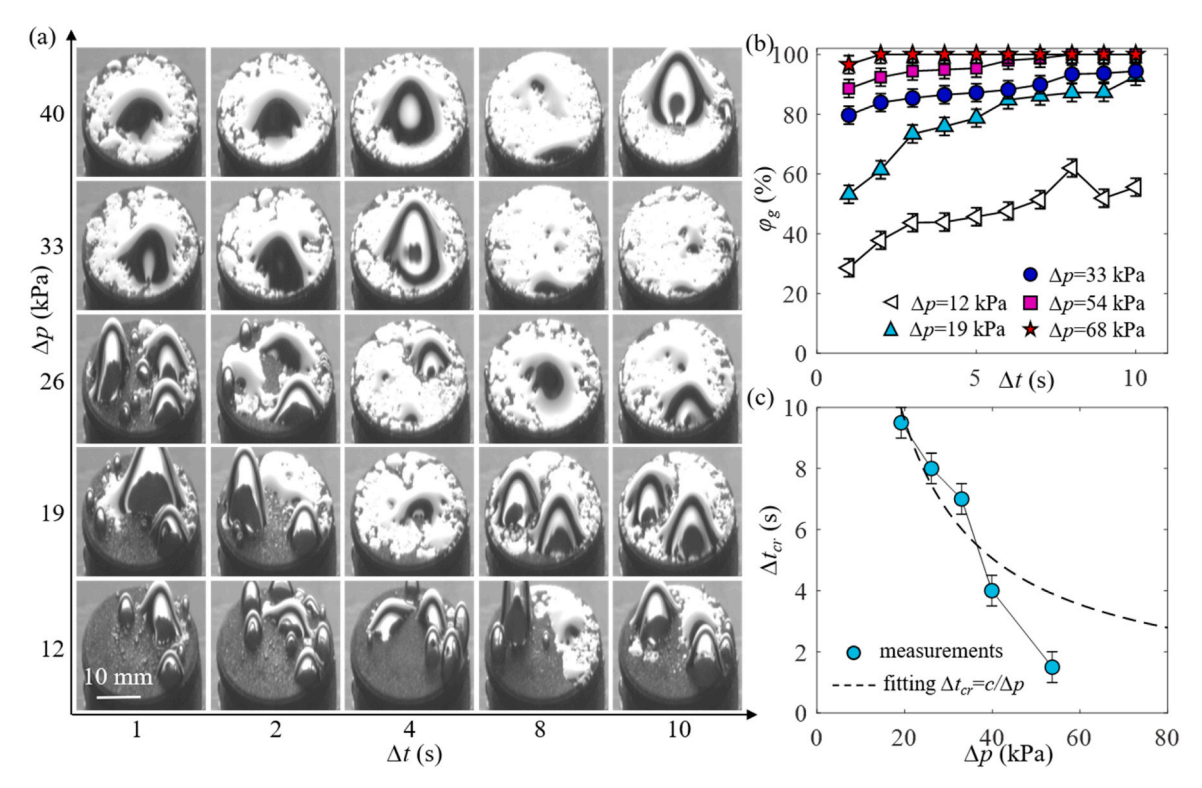


Fig. 6. (a) Status of the plastron on the surface shortly after the gas injection as a function the duration of gas injection ( $\Delta t$ ) and the pressure different ( $\Delta p$ ); (b) Percentage of surface area covered by gas ( $\varphi_g$ ) after gas injection test; (c) Critical gas injection duration ( $\Delta t_{cr}$ ) for achieving  $\varphi_g = 90$  % as a function of  $\Delta p$ .

cases, a single air bubble presented close to the center of the SHS, due to the residual air left on the surface after the gas injection. Results for  $\Delta p > 40\,$  kPa were similar to  $\Delta p = 40\,$  kPa and were therefore not included in Fig. 6(a).

To better quantify the degree of plastron restoration, we measured the percentage of surface area covered by gas and defined it as  $\varphi_8$ . To measure  $\varphi_8$ , we manually processed the images shown in Fig. 6(a) by selecting the regions that were not covered by gas, and then calculated  $\varphi_8$  as the ratio of gas-covered area to the total area. Fig. 6(b) plots  $\varphi_8$  as a function of  $\Delta t$  for different values of  $\Delta p$ . In all cases, an increase of  $\varphi_8$  with increasing  $\Delta t$  was observed. This trend was most obvious for cases where  $\Delta p$  was small. For example, as increasing  $\Delta t$  from 1 to 10 s,  $\varphi_8$  increased from 30 % to 50 % for the lowest  $\Delta p=12$  kPa, and from 50 % to 90 % at  $\Delta p=19$  kPa. At  $\Delta p=54$  kPa,  $\varphi_8$  was very close to 90 % at the smallest  $\Delta t=1$  s and increased to 100 % when  $\Delta t$  exceeded 8 s

Based on the trend in Fig. 6(b) that  $\varphi_g$  increased as increasing  $\Delta t$ , we defined a minimum duration of gas injection  $\Delta t_{cr}$  for which  $\varphi_g$  was larger than 90 %. Here, the threshold 90 % was arbitrarily selected. Fig. 6(c) shows  $\Delta t_{cr}$  as a function of  $\Delta p$ . As expected, increasing  $\Delta p$  led to a smaller  $\Delta t_{cr}$ . This result suggests that at a higher  $\Delta p$ , the plastron can be restored with a shorter duration of gas injection. Moreover, comparing the experimental data to the scaling  $\Delta t_{cr} \sim 1/\Delta p$  indicated that  $\Delta t_{cr}$  reduced at a rate faster than  $1/\Delta p$ .

### 3.2. Dynamic bubble formation and plastron restoration process

Next, to understand the dynamic process of how the plastron was restored, we showed the plastron restoration process at different levels of  $\Delta p$  while keeping  $\Delta t = 10$  s (the longest duration of gas injection). Fig. 7 and Supplementary Video 1 show a plastron restoration process by gas injection at  $\Delta p = 33$  kPa and  $\Delta t = 10$  s. Clearly, a short period after the gas injection has stopped (t = 13 s), the plastron on the entire SHS was restored. The plastron restoration process can be generally separated into three phases, as illustrated in Fig. 8. During Phase I (0 < t < 183 ms in Fig. 7), a number of micro-bubbles merged and randomly distributed on the SHS. It should be noted that we defined t = 0 as the time right before the presence of these tiny bubbles. The shape of these micro-bubbles was similar to these formed on an underwater orifice. These bubbles grew due to the gas flow. The growth rate varied at different positions, probably due to spatial variation of the porosity of the SHS. These bubbles could grow to a size of an order of O (1 mm) before merging with neighboring ones. We did not observe a detachment of these small bubbles probably because the surface tension force was larger than the buoyant force and momentum force.

During Phase II (183 ms < t < 10 s in Fig. 7), small bubbles grew, merged into large bubbles, and detached from the surface. We found two types of bubble merging: (i) merging of two bubbles that were directly contact with each other (e.g., t = 244 ms in Fig. 7), and (ii) merging of two non-contact bubbles that were separated at a certain distance (e.g.,

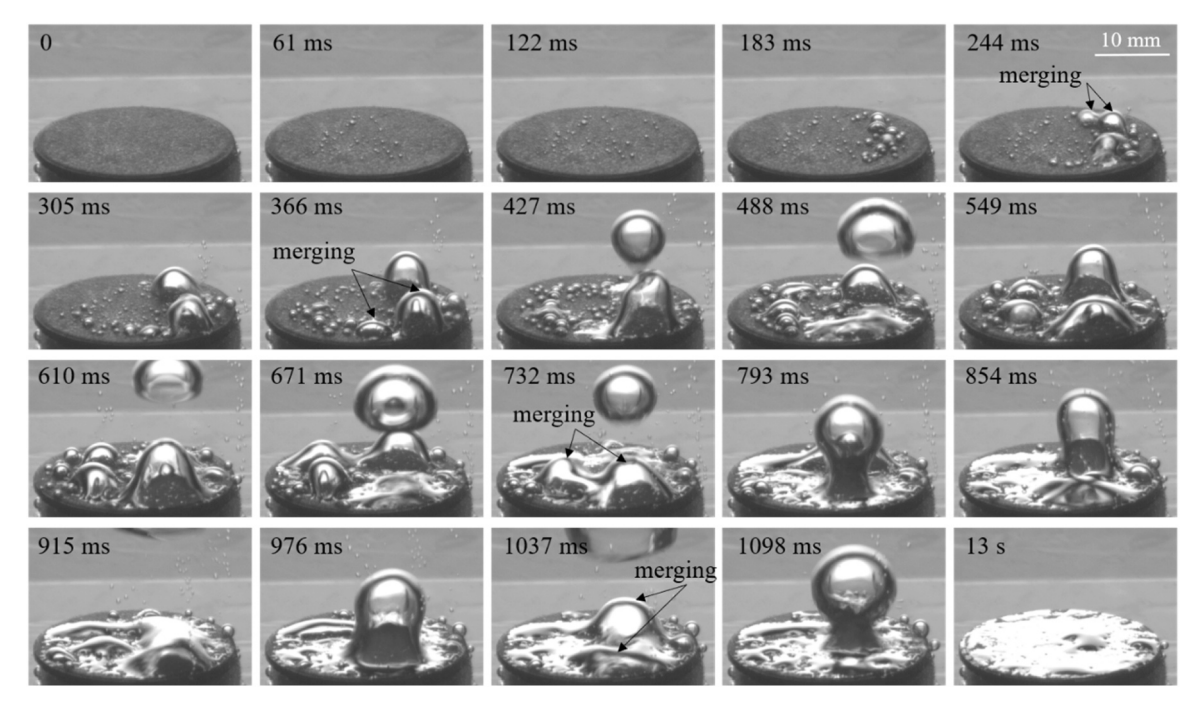


**Fig. 7.** Time-series of images showing the plastron restoration by gas injection with  $\Delta p = 33$  kPa and  $\Delta t = 10$  s. The final image (t = 13 s) was recorded a short period after gas injection had stopped. Multimedia view was provided in Supplementary Video 1.

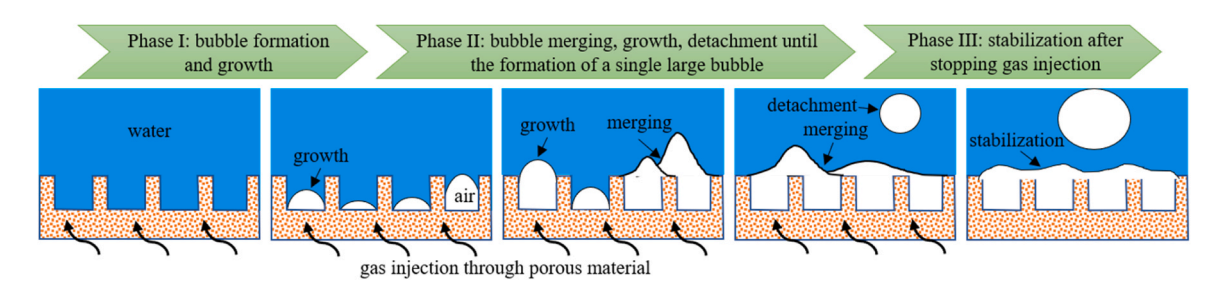


Fig. 8. Schematic representation of the plastron restoration process for underwater SHS by gas injection through porous material.

t = 366 ms in Fig. 7). In both cases, air flowed from the smaller bubbles to the larger ones, which had a smaller pressure inside the bubble according to the Young-Laplace equation. The latter case occurred due to the existence of a thin air layer on the surface, which bridged the two bubbles and promoted mass transfer between them, similar to these observed in other experiments [40,56]. The consequence of bubble merging was the formation of a bubble with a larger base, which increased the surface tension force and promoted the further bubble growth. The contact angle at the three-phase contact line was larger than 150° due to the hydrophobic coating. The merged bubbles kept growing until they formed a neck and detached from the surface when the buoyant and momentum forces overcame the surface tension force. A similar bubble growth with a large base radius on the SHS was observed in other studies [57,58]. Interestingly, immediately after the bubble detachment, an air layer was left at the same position on the surface. This was due to the superhydrophobic coating, which caused the air trapped Cassie-Baxter state to be thermodynamically favorable compared to the wetted Wenzel state [43]. As gas continued to be injected through the surface, at the position where the air layer was left, new air bubbles of a similar size to the detached ones repeatedly formed, grew, and detached. The coalescence of bubbles and the surface-tension effects during Phase II are reminiscent to the formation of complexes of attractive particles (such as DNA molecules) adsorbed on liquid interfaces [59-63].

During the early stage of Phase II (183 < t < 1037 ms in Fig. 7),

multiple air bubbles located at different positions along the SHS grew and detached. As time progressed, the bubbles further merged to bigger ones. At the late stage of Phase II ( $t>1098~\rm ms$ ), there was no further bubble merging. Only a single large bubble located at the center of surface repeatedly formed, grew, and detached. During Phase III after the gas injection has stopped ( $t>10~\rm s$ ), an uneven air layer covering the entire SHS was left on the surface and slowly stabilized to a thin, uniform layer under the influence of surface tension.

Fig. 9 and Supplementary Video 2 show the plastron restoration process at  $\Delta p=19$  kPa and  $\Delta t=10$  s. Due to the relatively low  $\Delta p,$  a small portion ( $\approx\!10$ %) of the SHS remained wetted following a short period after the gas injection. The gas pressure was not strong enough to displace all the liquid within the micro-pores on the surface. Yet, the overall plastron restoration process was similar to the one shown in Fig. 7. The key difference was at the late stage of Phase II. At low  $\Delta p,$  multiple small bubbles separated at certain distances, repeatedly formed, grew, and detached, without further merging to a single larger one. We found that the surface areas between these small bubbles remained wetted.

Fig. 10 and Supplementary Video 3 show the plastron restoration process at  $\Delta p=68$  kPa and  $\Delta t=10$  s. As expected, with a large  $\Delta p$ , the plastron over the entire SHS was restored shortly after the gas injection. The plastron restoration process followed similar steps as the schematic shown in Fig. 8. The merging of two non-contact bubbles (seen in Fig. 7) was also observed at t=98 ms and t=268 ms in Fig. 10. Compared to

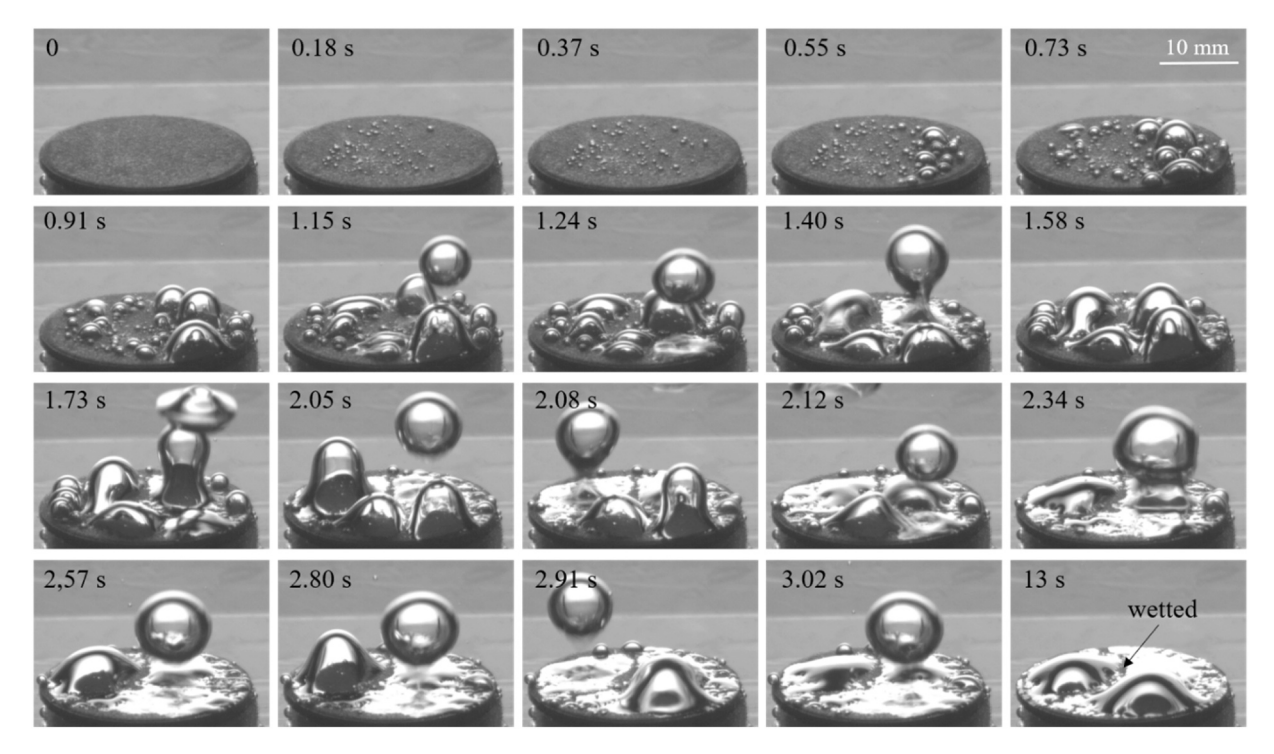
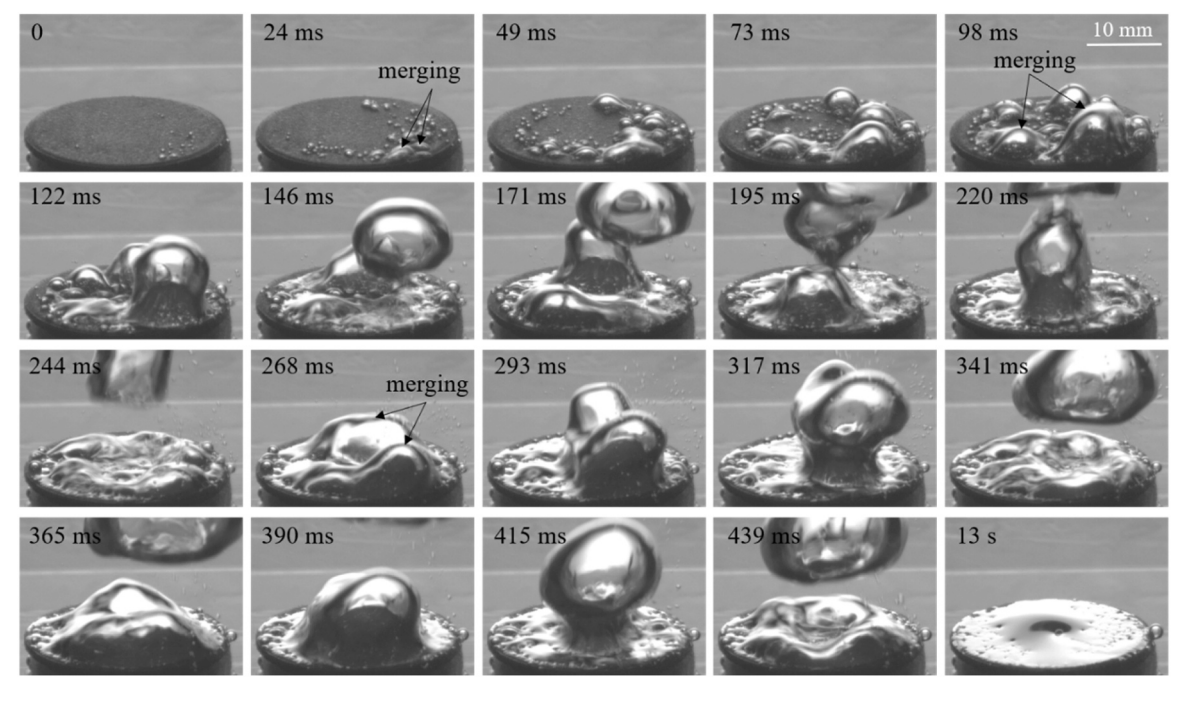


Fig. 9. Time-series of images showing the plastron restoration by gas injection with  $\Delta p = 19$  kPa and  $\Delta t = 10$  s. The final image (t = 13 s) was recorded a short period after gas injection had stopped. Multimedia view was provided in Supplementary Video 2.



**Fig. 10.** Time-series of images showing the plastron restoration by gas injection with  $\Delta p = 68$  kPa and  $\Delta t = 10$  s. The final image (t = 13 s) was recorded a short period after gas injection had stopped. Multimedia view was provided in Supplementary Video 3.

the low-pressure case shown in Fig. 7, the plastron restored at a much faster rate, including an earlier formation of micro-bubbles from the micro-pore on the SHS, a faster growth rate of gas bubbles, and the earlier merging of small bubbles to a single large bubble. Interestingly, we also found that the size of the bubbles detached from the SHS was larger compared to the one at the lower  $\Delta p$ .

To systemically investigate the impact of  $\Delta p$  on the plastron restoration process, we measured the time-variation of the diameter of the

detached bubbles  $D_b$ . Fig. 11(a) shows the time-variations of  $D_b$  for five different values of  $\Delta p$  in the range of 19–81 kPa. For large  $\Delta p$ , the detached bubbles were not perfectly spherical in shape,  $D_b$  was approximated by the horizonal dimension of the bubbles. For all cases, as increasing time,  $D_b$  gradually increased due to the merging of small bubbles at the early stage of plastron restoration before reaching to a stable value ( $D_b^{\text{stable}}$ ) when no more bubble merging occurred.

Fig. 11(b) shows the impact of  $\Delta p$  on the diameter of the bubble that

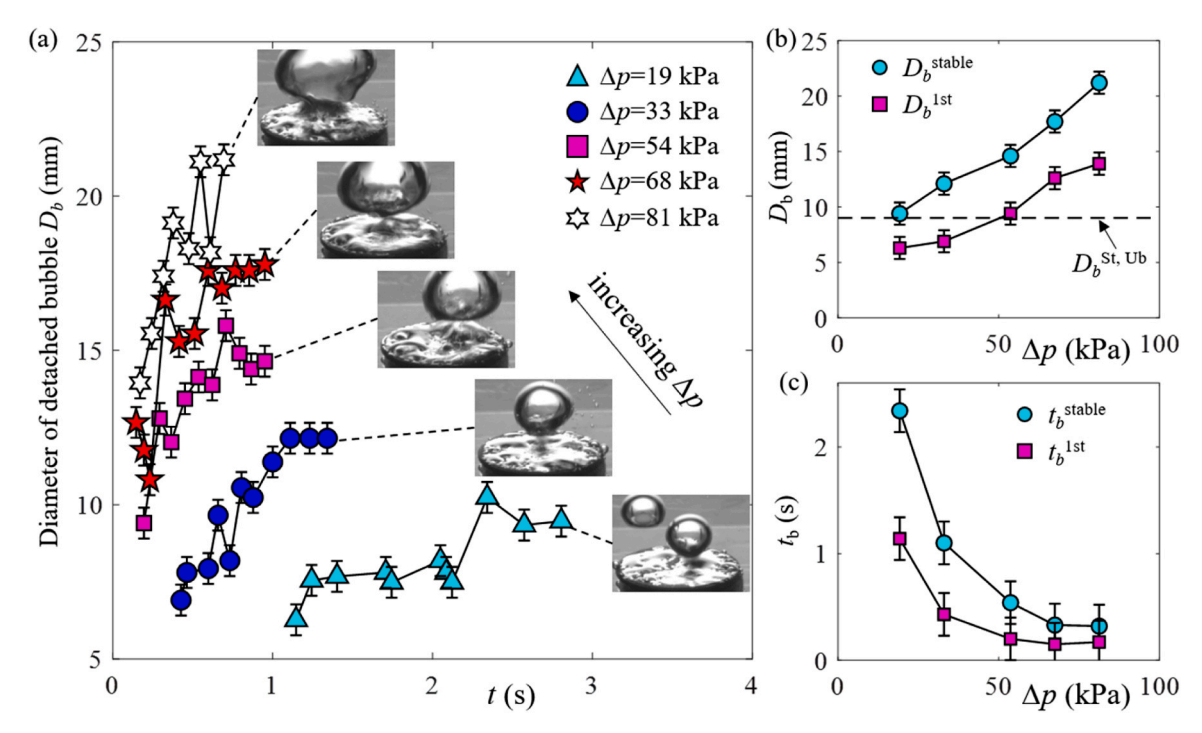


**Fig. 11.** (a) Time-variations of the diameter of bubble detached from the SHS ( $D_b$ ) at five different gas injection pressures; (b) Diameters for the first detached bubble ( $D_b^{\rm Ist}$ ) and for the detached bubble when  $D_b$  becames stable or when no more bubble merging occurred ( $D_b^{\rm stable}$ ) as a function of  $\Delta p$ ; and (c) Times for the first bubble to detach ( $t_b^{\rm Ist}$ ) and for  $D_b$  to become stable ( $t_b^{\rm stable}$ ) as a function of  $\Delta p$ .

firstly detached from SHS  $(D_b^{1st})$  as well as  $D_b^{stable}$ . We found that both  $D_b^{1st}$ and  $D_b^{\text{stable}}$  increased monotonically when  $\Delta p$  increased. Two possible reasons were identified for this trend. First, as  $\Delta p$  increased, the bubble base diameter ( $D_b^{\text{base}}$ ) increased, as can be seen by images shown in Figs. 7, 9 and 10. Since the surface tension force applied on the bubble equals to surface tension times the bubble base perimeter [58], a larger  $D_b^{\text{base}}$  led to an increase of the surface tension force, allowing the bubble to grow larger before the detachment. In the experimental studies by Rubio-Rubio et al. [58] and Qiao et al. [57], a larger detached bubble size due to an increase of  $D_b^{\text{base}}$  was also observed. In their experiments, different values of  $D_b^{\text{base}}$  were achieved by varying the size of the SHS. Here, the larger  $D_b^{\text{base}}$  was due to an increase of  $\Delta p$  and an increase of time. Second, the larger values of  $D_h^{1\text{st}}$  and  $D_h^{\text{stable}}$  could also be caused by the higher gas flow rates (Q) as increasing  $\Delta p$ . It is well known that for a bubble detaching from an orifice and at the dynamic region (when Q exceeds a critical flow rate  $Q_c$ ), the detached bubble size increases as increasing Q [64]. According to a model proposed by Oguz and Prosperetti [65],  $Q_c = \pi (16\sigma^5 R^5/3\rho^5 g^2)^{1/6}$ , where  $\sigma$  was the surface tension,  $R=D_h^{
m base}/2$  was the bubble base radius, ho was the density of liquid, and gwas the gravitational acceleration. Based on this model, for current maximum  $D_b^{\text{base}} = 20 \text{ mm}, Q_c = 885 \text{ ml/min}$ . As will be shown later, at the highest  $\Delta p = 81$  kPa, Q was found to be approximately 3500 ml/min which was larger than the value of  $Q_c$ .

For a comparison, the size of the bubble that detached from an unbounded SHS at the quasi-static region,  $D_b^{\mathrm{Sta,Ub}} = 9.1$  mm, deduced by Rubio-Rubio et al. [58] was also plotted in Fig. 11(b). At small  $\Delta p$ ,  $D_b^{\mathrm{Ist}}$  was smaller than  $D_b^{\mathrm{Sta,Ub}}$  since the SHS was not yet fully covered by air layer and the unbounded condition was not established yet. At large  $\Delta p$ , both  $D_b^{\mathrm{Ist}}$  and  $D_b^{\mathrm{Stable}}$  exceeded  $D_b^{\mathrm{Sta,Ub}}$  probably because the current flow rate belonged to the dynamic region as previously explained.

Fig. 11(c) shows the impact of  $\Delta p$  on the time when the first bubble detached from the surface  $(t_b^{\rm 1st})$ , and the time when  $D_b$  reached to a stable value  $(t_b^{\rm stable})$ . Here,  $t_b^{\rm 1st}$  and  $t_b^{\rm stable}$  could be approximated as the minimum duration of gas injection required for the plastron to be partially and fully recovered, respectively. In particular, injecting gas for a duration longer than  $t_b^{\rm stable}$  will not significantly improve  $\varphi_g$ . As shown

in Fig. 11(c), as increasing  $\Delta p$  from 19–81 kPa, both  $t_b^{\rm 1st}$  and  $t_b^{\rm stable}$  quickly reduced and reached to stable values of about 0.15 s and 0.32 s, respectively. For a comparison, the in-situ gas generation techniques required more than 20 s for the plastron to be restored [40,43]. The reason that  $t_b^{\rm 1st}$  and  $t_b^{\rm stable}$  reduced as increasing  $\Delta p$  included the faster merging of small bubbles and the larger gas flow rate. However, the reason that  $t_b^{\rm 1st}$  and  $t_b^{\rm stable}$  did not further reduce at  $\Delta p > 68$  kPa was unclear, and required future studies.

We also performed an experiment for gas injection through an uncoated, hydrophilic porous disk. The result was shown in Fig. 12 and Supplementary Video 4. The process of bubble formation, growth, and detachment was very different from the coated porous disk or the SHS. Unlike the coated one, each time after a bubble detached from the uncoated surface, no air layer was left behind on the surface. The size of detached bubble was about 2–3 mm, much smaller compared to these detached from the SHS. A merging of two non-contact bubbles separated at a short distance, as seen for the coated porous disk, was not observed here.

### 3.3. Gas flow rate during the plastron restoration process

To better understand how gas passed through the porous SHS during the plastron restoration process, we calculated the gas flow rate as:

$$Q(t) = \frac{\delta V}{\delta t} = \frac{\pi D_b^{n3}/6}{t_h^n - t_h^{n-1}},$$
 (2)

where  $\delta V = \pi D_b^{n3}/6$  is the volume of gas (or volume of bubble) passed through the surface during a time duration  $\delta t = t_b^n - t_b^{n-1}$ ,  $D_b^n$  denotes the diameter of the  $n^{th}$  bubble detached from the surface,  $t_b^n$  and  $t_b^{n-1}$  denote the time when the  $n^{th}$  and  $(n-1)^{th}$  bubble detached from the surface (noted  $t^{n=0}=0$ ). Noted that this method might under- or over-estimate the value of Q for low  $\Delta p$  since multiple bubbles grew and detached from the surface, and only the volume of a single bubble was account at a time. The magnitude of Q was an important parameter because it determined whether the bubble formation process was at the quasi-static regime or at the dynamic regime [64]. Fig. 13(a) shows the

Fig. 12. Time-series of images showing the bubble restoration from an un-coated, hydrophilic porous material by gas injection with  $\Delta p = 5$  kPa. Multimedia view was provided in Supplementary Video 4.

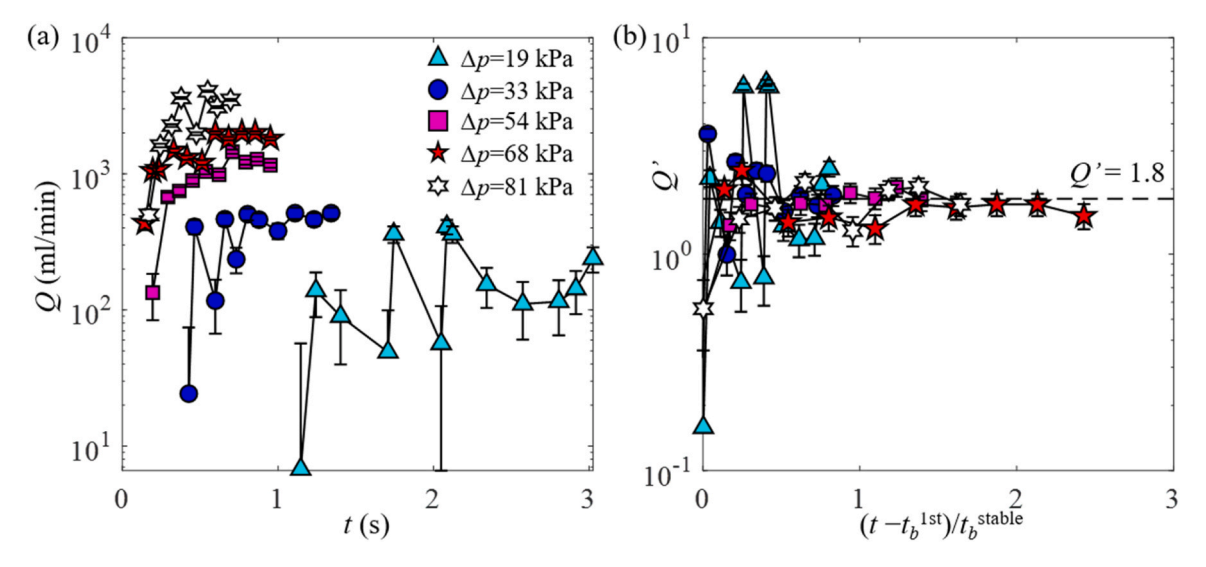


Fig. 13. (a) Time-variations of gas flow rates at five different gas injection pressures; and (b) Normalized gas flow rates.

time-variations of Q corresponding to the five cases shown in Fig. 11(a). The magnitude of Q fell within the range of 10–3500 ml/min with the upper limit belonging to the dynamic regime as explained earlier. As expected, in agreement with the Darcy's law, Q increased as increasing  $\Delta p$ . Moreover, we found that for all cases, Q initially increased with time and then became stable.

To explain the observed trends for Q, we defined and calculated a dimensionless flow rate  $Q^{\prime}$  as:

$$Q' = \frac{Q}{k\Delta p D_b^2/\mu L}. (3)$$

This equation is inspired from Eq. (1) where Q has a unit of  $k\Delta pA/\mu L$ . For the permeability in Eq. (3), we used  $k=2.7\times10^{-14}$  m<sup>2</sup>, a value measured when both sides of the SHS were exposed to air (see Fig. 3). We also replaced the surface area A as  $D_b^2$ . Fig. 13(b) shows the timevariations of Q'. Interestingly, after the normalization, all of the profiles collapsed nicely, having a value close to Q'=1.8. Substituting Q'=1.8 into Eq. (3), we obtained the following relation:

$$Q \approx 1.8 \frac{kD_b^2}{\mu} \frac{\Delta p}{L}.$$
 (4)

Eq. (4) is very similar to the Eq. (1), suggesting that the flow of air through the underwater porous SHS followed a modified Darcy's law. The difference between the two equations is that in Eq. (4) Q is proportional to  $D_b^2$  (the cross-section area of the bubble), but in Eq. (1) Q is proportional to A (the surface area of the porous plate). This difference can be explained as following: when both sides of the porous SHS are exposed to air, the surface area allowing gas to pass through is simply A; while when one side of the porous SHS was submerged underwater, the area allowing gas to pass through scales with  $D_b^2$ . Eq. (4) is useful since it can be applied to predict the gas flow rate across the porous SHS when it is submerged in water. According to the proposed Eq. (4), the reason Q

increased with time was due to the increase of  $D_b^2$ . It is also worth noting that the permeability for the porous SHS with one side exposed to water was nearly same to the permeability for the SHS with both sides were exposed to air. Future studies are needed to understand the underlying mechanism of this phenomenon.

### 4. Conclusions

In summary, we developed and demonstrated a technique to restore the plastron on an underwater superhydrophobic surface. The technique was based on the principle of creating SHS on a porous base and subsequently restoring the plastron by gas injection. The experiments started from a condition where all the gas on SHS was removed. First, we studied the impacts of gas injection pressure  $\Delta p$  and gas injection duration  $\Delta t$  on the degree of plastron restoration. We found that the percentage of surface area being recovered with a uniform air layer increased with increasing  $\Delta p$  and  $\Delta t$ . When  $\Delta p$  and  $\Delta t$  were sufficiently large, the entire SHS was recovered with an air layer. It is the first experimental study that demonstrated the capability of using gas injection and porous material to restore plastron from a fully wetted state.

Furthermore, we provided a first experimental study showing the dynamic process of bubble formation and plastron restoration by using high-speed imaging. We found that the plastron restoration process typically involved the formation, merging, growth, and detachment of gas bubbles. Immediately after the detachment of bubbles, a layer of gas was left on the surface. The size of the detached bubbles initially increased with time and then became stable when there was no further bubble merging. Increasing  $\Delta p$  caused a larger gas flow rate, a larger detached bubble size, and an earlier bubble detachment and plastron restoration. At the highest pressure, a plastron restoration within 0.3 s was achieved, faster than the in-situ gas generation techniques. The gas flow rate through the underwater SHS can be described by a modified Darcy's law, where the surface area was replaced by the area of detached

bubble and the permeability was similar to the one measured when both sides of SHS were exposed to air.

Future studies are required to understand the impacts other parameters on the plastron restoration, including Reynolds number of external flows, permeability of the porous material, and texture geometry of the SHS. Future studies are also needed to gain a deeper understanding of the bubble formation on the porous SHS.

### CRediT authorship contribution statement

**Jordan Breveleri:** Data curation, Investigation, Formal analysis, Writing – original draft. **Shabnam Mohammadshahi:** Investigation, Writing – review & editing. **Theresa Dunigan:** Investigation, Writing – review & editing. **Hangjian Ling:** Conceptualization, Funding acquisition, Supervision, Writing – review & editing.

# **Declaration of Competing Interest**

The authors declare that they have no known competing financial interests or personal relationships that could have appeared to influence the work reported in this paper.

### **Data Availability**

The data that support the findings of this study are available from the corresponding author upon reasonable request.

### Acknowledgments

We thank the support of National Science Foundation under Grant No. 2041479 and No. 2149893, UMass Dartmouth's Marine and Undersea Technology (MUST) Research Program funded by the Office of Naval Research (ONR) under Grant No. N00014-20-1-2170, and Seed Funding program from the Office of the Provost at the University of Massachusetts Dartmouth.

### References

- [1] J.P. Rothstein, Slip on superhydrophobic surfaces, Annu. Rev. Fluid Mech. 42 (2010) 89–109.
- [2] C. Lee, C.H. Choi, C.J. Kim, Superhydrophobic drag reduction in laminar flows: a critical review, Exp. Fluids 57 (2016) 1–20.
- [3] X. Zhao, A. Best, W. Liu, K. Koynov, H.J. Butt, C. Schönecker, Irregular, nanostructured superhydrophobic surfaces: local wetting and slippage monitored by fluorescence correlation spectroscopy, Phys. Rev. Fluids 6 (2021) 1–25.
- [4] H. Park, C.-H. Choi, C.-J. Kim, Superhydrophobic drag reduction in turbulent flows: a critical review, Exp. Fluids 62 (2021) 229.
- [5] G.B. Hwang, K. Page, A. Patir, S.P. Nair, E. Allan, I.P. Parkin, The anti-biofouling properties of superhydrophobic surfaces are short-lived, ACS Nano 12 (2018) 6050–6058.
- [6] X. Chang, M. Li, S. Tang, L. Shi, X. Chen, S. Niu, X. Zhu, D. Wang, S. Sun, Superhydrophobic micro-nano structured PTFE/WO3 coating on low-temperature steel with outstanding anti-pollution, anti-icing, and anti-fouling performance, Surf. Coat. Technol. 434 (2022), 128214.
- [7] X. Wang, Y. Liu, H. Cheng, X. Ouyang, Surface wettability for skin-interfaced sensors and devices, Adv. Funct. Mater. 32 (2022) 2200260.
- [8] Y. Liu, Z. Sheng, J. Huang, W. Liu, H. Ding, J. Peng, B. Zhong, Y. Sun, X. Ouyang, H. Cheng, X. Wang, Moisture-resistant MXene-sodium alginate sponges with sustained superhydrophobicity for monitoring human activities, Chem. Eng. J. 432 (2022).
- [9] Y. Liu, X. Li, H. Yang, P. Zhang, P. Wang, Y. Sun, F. Yang, W. Liu, Y. Li, Y. Tian, S. Qian, S. Chen, H. Cheng, X. Wang, Skin-Interfaced superhydrophobic insensible sweat sensors for evaluating body thermoregulation and skin barrier functions, ACS Nano 17 (2023) 5588–5599.
- [10] Y. Zhang, Y. Chen, J. Huang, Y. Liu, J. Peng, S. Chen, K. Song, X. Ouyang, H. Cheng, X. Wang, Skin-interfaced microfluidic devices with one-opening chambers and hydrophobic valves for sweat collection and analysis, Lab Chip 20 (2020) 2635–2645.
- [11] N. Yu, Z.R. Li, A. McClelland, F.J. del Campo Melchor, S.Y. Lee, J.H. Lee, C.J. Kim, Sustainability of the plastron on nano-grass-covered micro-trench superhydrophobic surfaces in high-speed flows of open water, J. Fluid Mech. 962 (2023) A9.

- [12] Y.A. Mehanna, E. Sadler, R.L. Upton, A.G. Kempchinsky, Y. Lu, C.R. Crick, The challenges, achievements and applications of submersible superhydrophobic materials, Chem. Soc. Rev. 50 (2021) 6569–6612.
- [13] S. Huang, P. Lv, H. Duan, Morphology evolution of liquid–gas interface on submerged solid structured surfaces, Extrem. Mech. Lett. 27 (2019) 34–51.
- [14] J. Hyväluoma, J. Harting, Slip flow over structured surfaces with entrapped microbubbles, Phys. Rev. Lett. 100 (2008), 246001.
- [15] P. Gao, J.J. Feng, Enhanced slip on a patterned substrate due to depinning of contact line, Phys. Fluids 21 (2009), 102102.
- [16] J.S. Wexler, I. Jacobi, H.A. Stone, Shear-driven failure of liquid-infused surfaces, Phys. Rev. Lett. 114 (2015) 1–5.
- [17] J. Seo, R. García-Mayoral, A. Mani, Pressure fluctuations and interfacial robustness in turbulent flows over superhydrophobic surfaces, J. Fluid Mech. 783 (2015) 448–473.
- [18] J. Seo, R. García-Mayoral, A. Mani, Turbulent flows over superhydrophobic surfaces: flow-induced capillary waves, and robustness of air-water interfaces, J. Fluid Mech. 835 (2018) 45–85.
- [19] D. Reholon, S. Ghaemi, Plastron morphology and drag of a superhydrophobic surface in turbulent regime, Phys. Rev. Fluids 3 (2018) 1–21.
- [20] H. Ling, J. Katz, M. Fu, M. Hultmark, Effect of Reynolds number and saturation level on gas diffusion in and out of a superhydrophobic surface, Phys. Rev. Fluids 2 (2017), 124005.
- [21] B.V. Hokmabad, S. Ghaemi, Effect of flow and particle-plastron collision on the longevity of superhydrophobicity, Sci. Rep. 7 (2017) 41448.
- [22] H. Kim, H. Park, Diffusion characteristics of air pockets on hydrophobic surfaces in channel flow: three-dimensional measurement of air-water interface, Phys. Rev. Fluids 4 (2019), 074001.
- [23] P. Papadopoulos, L. Mammen, X. Deng, D. Vollmer, H.-J. Butt, How superhydrophobicity breaks down, Proc. Natl. Acad. Sci. USA 110 (2013) 3254–3258.
- [24] Q.-S. Zheng, Y. Yu, Z.-H. Zhao, Effects of hydraulic pressure on the stability and transition of wetting modes of superhydrophobic surfaces, Langmuir 21 (2005) 12207–12212.
- [25] C.W. Extrand, Repellency of the lotus leaf: resistance to water intrusion under hydrostatic pressure, Langmuir 27 (2011) 6920–6925.
- [26] S. Mohammadshahi, J. Breveleri, H. Ling, Fabrication and characterization of super-hydrophobic surfaces based on sandpapers and nano-particle coatings, Colloids Surf. A Physicochem. Eng. Asp. 666 (2023), 131358.
- [27] Y. Kwon, N. Patankar, J. Choi, J. Lee, Design of surface hierarchy for extreme hydrophobicity, Langmuir 25 (2009) 6129–6136.
- [28] C. Lee, C.J. Kim, Maximizing the giant liquid slip on superhydrophobic microstructures by nanostructuring their sidewalls, Langmuir 25 (2009) 12812–12818.
- [29] J. Zhang, Z. Yao, P. Hao, Drag reductions and the air-water interface stability of superhydrophobic surfaces in rectangular channel flow, Phys. Rev. E 94 (2016), 053117.
- [30] T. Verho, J.T. Korhonen, L. Sainiemi, V. Jokinen, C. Bower, K. Franze, S. Franssila, P. Andrew, O. Ikkala, R.H.A. Ras, Reversible switching between superhydrophobic states on a hierarchically structured surface, Proc. Natl. Acad. Sci. USA 109 (2012) 10210–10213.
- [31] Y. Xue, S. Chu, P. Lv, H. Duan, Importance of hierarchical structures in wetting stability on submersed superhydrophobic surfaces, Langmuir 28 (2012) 9440–9450.
- [32] S. Heo, W. Choi, S.J. Lee, Enhanced air stability of ridged superhydrophobic surface with nanostructure, AIP Adv. 11 (2021), 105209.
- [33] A. Tuteja, W. Choi, M. Ma, J.M. Mabry, S.A. Mazzella, G.C. Rutledge, G. H. McKinley, R.E. Cohen, Designing superoleophobic surfaces, Sciences (80-.) 318 (2007) 1618–1622.
- [34] M. Xu, A. Grabowski, N. Yu, G. Kerezyte, J. Lee, B.R. Pfeifer, C.J. Kim, Superhydrophobic drag reduction for turbulent flows in open water, Phys. Rev. Appl. 13 (2020), 034056.
- [35] P. Sun, X. Feng, G. Tian, X. Zhang, J. Chu, Ultrafast self-healing superhydrophobic surface for underwater drag reduction, Langmuir 38 (2022) 10875–10885.
- [36] D. Gandyra, S. Walheim, S. Gorb, P. Ditsche, W. Barthlott, T. Schimmel, Air retention under water by the floating fern salvinia: the crucial role of a trapped air layer as a pneumatic spring, Small 16 (2020).
- [37] O. Tricinci, T. Terencio, B. Mazzolai, N.M. Pugno, F. Greco, V. Mattoli, 3D micropatterned surface inspired by salvinia molesta via direct laser lithography, ACS Appl. Mater. Interfaces 7 (2015) 25560–25567.
- [38] R.N. Wenzel, Resistance of solid surfaces to wetting by water, Ind. Eng. Chem. 28 (1936) 988–994.
- [39] A.B.D. Cassie, S. Baxter, Wettability of porous surfaces, Trans. Faraday Soc. 40 (1944) 546–551.
- [40] C. Lee, C.J. Kim, Underwater restoration and retention of gases on superhydrophobic surfaces for drag reduction, Phys. Rev. Lett. 106 (2011) 1–4.
- 41] B.P. Lloyd, P.N. Bartlett, R.J.K. Wood, Active gas replenishment and sensing of the wetting state in a submerged superhydrophobic surface, Soft Matter 13 (2017) 1413–1419.
- [42] J. Lee, K. Yong, Combining the lotus leaf effect with artificial photosynthesis: Regeneration of underwater superhydrophobicity of hierarchical ZnO/Si surfaces by solar water splitting, NPG Asia Mater. 7 (2015) 1–9.
- [43] D. Panchanathan, A. Rajappan, K.K. Varanasi, G.H. McKinley, Plastron regeneration on submerged superhydrophobic surfaces using in situ gas generation by chemical reaction, ACS Appl. Mater. Interfaces 10 (2018) 33684–33692.
- [44] I.U. Vakarelski, D.Y.C. Chan, J.O. Marston, S.T. Thoroddsen, Dynamic air layer on textured superhydrophobic surfaces, Langmuir 29 (2013) 11074–11081.

- [45] D. Dilip, N.K. Jha, R.N. Govardhan, M.S. Bobji, Controlling air solubility to maintain "Cassie" state for sustained drag reduction, Colloids Surf. A Physicochem. Eng. Asp. 459 (2014) 217–224.
- [46] I.U. Vakarelski, N.A. Patankar, J.O. Marston, D.Y.C. Chan, S.T. Thoroddsen, Stabilization of Leidenfrost vapour layer by textured superhydrophobic surfaces, Nature 489 (2012) 274–277.
- [47] D. Saranadhi, D. Chen, J.A. Kleingartner, S. Srinivasan, R.E. Cohen, G.H. McKinley, Sustained drag reduction in a turbulent flow using a low-Temperature Leidenfrost surface, Sci. Adv. 2 (2016).
- [48] P. Du, J. Wen, Z. Zhang, D. Song, A. Ouahsine, H. Hu, Maintenance of air layer and drag reduction on superhydrophobic surface, Ocean Eng. 130 (2017) 328–335.
- [49] Y. Zhao, Z. Xu, L. Gong, S. Yang, H. Zeng, C. He, D. Ge, L. Yang, Recoverable underwater superhydrophobicity from a fully wetted state via dynamic air spreading, iScience 24 (2021), 103427.
- [50] W. Cho, S. Heo, S.J. Lee, Effects of surface air injection on the air stability of superhydrophobic surface under partial replenishment of plastron, Phys. Fluids 34 (2022), 122115.
- [51] S. Qin, H. Fang, S. Sun, X. Wang, L. Cao, D. Wu, Fabrication of air-permeable superhydrophobic surfaces with excellent non-wetting property, Mater. Lett. 313 (2022), 131783.
- [52] H. Ling, S. Srinivasan, K. Golovin, G.H. McKinley, A. Tuteja, J. Katz, Highresolution velocity measurement in the inner part of turbulent boundary layers over super-hydrophobic surfaces, J. Fluid Mech. 801 (2016) 670–703.
- [53] Z. Li, J. Marlena, D. Pranantyo, B.L. Nguyen, C.H. Yap, A porous superhydrophobic surface with active air plastron control for drag reduction and fluid impalement resistance, J. Mater. Chem. A 7 (2019) 16387–16396.
- [54] M. Zhang, H. Hu, J. Wen, L. Ren, L. Xie, Controlling the morphology and slippage of the air-water interface on superhydrophobic surfaces, Exp. Fluids 64 (2023) 121

- [55] S. Whitaker, Flow in porous media I: a theoretical derivation of Darcy's law, Transp. Porous Media 1 (1986) 3–25.
- [56] F.M. Chang, Y.J. Sheng, S.L. Cheng, H.K. Tsao, Tiny bubble removal by gas flow through porous superhydrophobic surfaces: Ostwald ripening, Appl. Phys. Lett. 92 (2008) 1–4.
- [57] S. Qiao, C. Cai, W. Chen, C. Pan, Y. Liu, Control of the shape of bubble growth on underwater substrates with different sizes of superhydrophobic circles, Phys. Fluids 34 (2022), 067110.
- [58] M. Rubio-Rubio, R. Bolaños-Jiménez, C. Martínez-Bazán, J.C. Muñoz-Hervás, A. Sevilla, Superhydrophobic substrates allow the generation of giant quasi-static bubbles, J. Fluid Mech. 912 (2021) A25.
- [59] A.G. Cherstvy, E.P. Petrov, Modeling DNA condensation on freestanding cationic lipid membranes, Phys. Chem. Chem. Phys. 16 (2014) 2020–2037.
- [60] L. Barberi, F. Livolant, A. Leforestier, M. Lenz, Local structure of DNA toroids reveals curvature-dependent intermolecular forces, Nucleic Acids Res. 49 (2021) 3709–3718.
- [61] A. Khmelinskaia, H.G. Franquelim, R. Yaadav, E.P. Petrov, P. Schwille, Membrane-mediated self-organization of rod-like DNA origami on supported lipid bilayers, Adv. Mater. Interfaces 8 (2021) 2101094.
- [62] A. Leforestier, F. Livolant, Structure of toroidal DNA collapsed inside the phage capsid, Proc. Natl. Acad. Sci. USA 106 (2009) 9157–9162.
- [63] A.G. Cherstvy, Structure of DNA toroids and electrostatic attraction of DNA duplexes, J. Phys. Condens. Matter 17 (2005) 1363.
- [64] A.A. Kulkarni, J.B. Joshi, Bubble formation and bubble rise velocity in gas—liquid systems: a review, Ind. Eng. Chem. Res. 44 (2005) 5873–5931.
- [65] H.N. Oguz, A. Prosperetti, Dynamics of bubble growth and detachment from a needle, J. Fluid Mech. 257 (1993) 111.